Chapter 6

# Spectroscopic Investigations on Polyvinyl Alcohol Film with Complex of Terbium Ions along with Bismuth Nanoparticles for Improved Green Emission

Gagandeep Kaur, Brijesh Kumar and S.B. Rai

Additional information is available at the end of the chapter

http://dx.doi.org/10.5772/intechopen.70274

**Abstract**

In this chapter, bismuth nanoparticles (NPs) have been synthesized by the pulsed laser ablation technique at different pH in different aqueous solutions (namely, water (H), water + sodium hydroxide (HN), and water + hydrochloric acid (HC)). The NPs in aqueous solutions have been characterized by transmission electron microscopy (TEM) and UV-Vis-NIR absorption techniques. The NPs are spherical, core shell, and hollow spheres in H, HN, and HC, respectively. The vibrational features have been studied using Raman technique and correlated with solid NPs, hollow NPs, core shell NPs, and NPs complex, etc. The Bi NPs were subsequently scattered with $Tb^{3+}$ ions and their complex with salicylic acid (Sal) and 1,10-phenanthroline in aqueous solution of polyvinyl alcohol to get thin polymer films. Then photoluminescence properties of $Tb^{3+}$ ions and the $(Tb(Sal)_3(Phen))$ complex were studied using 266 nm and 355 nm as excitation wavelengths to seek into the influence of Bi NPs on their emissive properties. Terbium ions in case of $(Tb(Sal)_3(Phen))$ complex together with NPs demonstrate an intense and extended emission spectrum in the 375–700 nm range for transition arising even from $^5D_3$ and $^5D_4$ levels to different $^7F_J$ levels on 266 nm excitation. Alternatively, the luminescence intensity of $Tb^{3+}$ ions complexed with Sal and Phen in the thin polymer films is improved appreciably as compared with $Tb^{3+}$ ions in the presence of Bi NPs on excitation with 355 nm.

**Keywords:** nanoparticles, laser processing, polymers, luminescence, thin films

## 1. Introduction

Optically active materials doped with lanthanide (RE) ions dispersed in polymer are appropriate for use in a diversity of optoelectronic applications such as amplifiers, fibers, and

waveguides due to their stumpy expenditure and simplicity of processing and lofty performance [3, 13]. RE ions offer intense narrow spectral emissions from the long-lived excited-states arising from partially filled $4f^n$ orbitals [19]. When supplemented with the polymer host, these favorable radiative properties of RE ions have a tendency to get diminished by the intrinsic soaring vibrational frequencies of different bonds of polymers. Moreover, RE ion salts exhibit limited solubility in polymers and tend to aggregate, resulting in enhanced scattering and luminescence quenching even at low concentrations. Consequently, RE ions are united with an organic ligand before being dispersed in polymeric hosts to circumvent this. These organic ligands absorb the incident light energy and transfer it to the RE ion and can act as antenna ligands as shown in **Figure 1**.

The encapsulation of the RE ion is done with an appropriate organic ligand that is capable of transferring the input energy absorbed by the ligand to the RE ion. The triply ionized RE ions can be complexed with diverse types of strongly absorbing chelating ligands, e.g., β-diketones bipyridines, cryptands, calixarenes, cyclodextrins, and crown ethers [23]. Such complexed systems have large solubility in a lot of common organic solvents, such as chloroform, benzene, toluene, and are also soluble in several polymer matrices. One such ligand is salicylic acid (here after Sal), which is naturally prevalent as its glucosides in willow leaves and poplar, and birch. It is commonly recognized as ortho hydroxybenzoic acid or 2-hydroxybenzoic acid. Major component from the manufacture of salicylic acid is used in the production of aspirin (acetylsalicylic acid) nowadays. Molecular structure of salicylic acid is shown in **Figure 2**. The crystal structure of salicylic acid is monoclinic and has been resolved by Cochran. The crystal structure of salicylic acid is centro-symmetric carboxylic acid dimers. The hydroxyl group is hydrogen bonded intra-molecularly to the carbonyl oxygen. This leads to a less flexible molecule and dimer and a reduced intermolecular hydrogen bonding. The sensitized luminescence of lanthanide ions (especially $Tb^{3+}$ ion by salicylic acid (Sal) has been found to play an important role in the analytical chemistry for the analysis of trace amount of Sal and its derivatives in biological systems. Kaur et al. [20] have prepared terbium complexes with salicylic acid and observed enhanced luminescence properties of terbium ion. RE(III) ions are chelated with ligands that have broad intense absorption bands. In these systems, intense ion luminescence originates from the intramolecular energy transfer

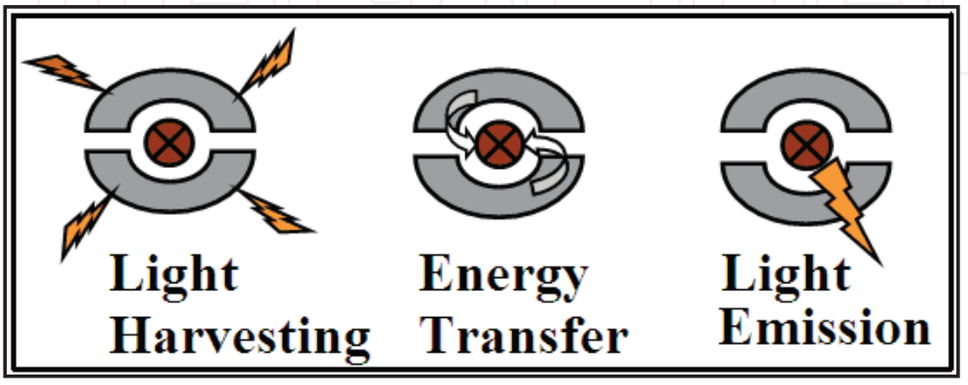


**Figure 1.** Pictorial representation of antenna effect.

http://dx.doi.org/10.5772/intechopen.70274

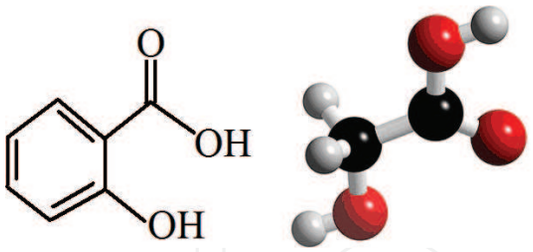


**Figure 2.** The structure of salicylic acid.

through the excited state of the ligand to the emitting level of the RE(III) ion. Salicylic acid is an effective aromatic carboxylic acid, also known as ligand transferring energy to the lanthanide ions. The sensitization of Tb(III) luminescence by the salicylic acid and its derivatives were also used for determination of salicylic acid in biological applications.

Thus, RE coordinated complexes in polymer hosts are used for numerous practical applications and their luminescence efficiency may be improved by a variety of methods [3, 4, 13, 20, 22]. Besides the sensitization by organic ligands, the fluorescence of the lanthanides in the complexes can be further enhanced by the use of synergistic agents, which provide an insulating layer around the lanthanide complex, reducing the probability of radiationless energy transfer from the complex to the solvent. In addition, these are usually adopted to expel adsorbed water from the first coordination sphere and thus enhance luminescence as water molecules quench the luminescence through radiationless deactivation. Recently, synergetic ligands have been used to control the supermolecular structure of rare earth complexes and grafted the RE complex in the host matrix to form homogeneous stable functional materials and different synergetic ligands such as trioctylphosphine oxide (TOPO), thenoyltrifluoroacetonatone (TTA), tripenylphosphine oxide (TPPO), 1,10-phenanthroline (Phen), 2,2-bipy (Dipy), trioctylphosphine (TOPO), etc. We have used 1,10-phenanthroline (Phen) for our investigations—10-phenanthroline (Phen) is a heterocyclic organic compound and a bidentate ligand. It forms a strong complex with most metal ions. The molecular formula of Phen is $C_{12}H_8N_2$, and the chemical structures of some such ligands are shown in **Figure 3**. Any effort to improve the efficiency by increasing the RE concentration does not succeed, as aggregation of ions takes place at higher concentrations and these acts as quenching centers.

Nanoparticles (NPs) are emerging as interesting luminescent nanoscale materials not only for basic research but also for numerous applications in varied devices such as optical amplifiers, color displays, solid-state lasers, etc. The NPs affect the luminescence and dynamics of optically energetic lanthanide ions. Occurrence of enhanced intensity of emission is correlated

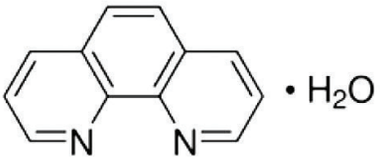


**Figure 3.** The structure of 1,10-phenanthroline ligand.

by means of energy transfer amid nanoparticles and the active rare earth ions. The second available option for the augmentation effect is via local energy field of NPs acting on the lanthanide ions positioned in their propinquity. This effect is prominent in particular when there is a matching of the surface plasmon resonance wavelength of the NPs and the incident light beam wavelength or luminescence wavelength [7, 26]. High surface-to-volume ratio and local phenomena such as absorption or changes in the surface electronic state may contribute significantly to special properties.

Metallic and semimetallic NPs are striking examples to be explored nowadays. The phenomenon of quantum size effect has a great influence on the physical properties that are very different from those of the bulk ones. Bismuth is a semimetal with a small energy overlap between the conduction and the valence bands. The size-induced semimetal to semiconductor transition and the related quantum confinement effects are potentially useful for optical and electro-optical device applications [2, 10, 16, 36, 37]. It has a high carrier mobility, a highly anisotropic Fermi surface, and miniature effective mass [2, 24, 46]. Below the size of 30 nm, the Bi NPs behave as semiconductors [44]. The formations of semimetal to semiconductor materials are being used in different scientific devices such as in optic and electro optic devices [39]. Bi NPs exhibit absorption in the UV region [27–29, 43]. The absorption peak shifts toward lower wavelengths in the case of smaller Bi NPs and, vice versa. The stability of Bi NPs decreases with a decrease in its particle size (due to enhanced surface to volume ratio). Nevertheless, these demonstrate strong reactive morphology. There are various methods to produce NPs. Among the diverse techniques used to fabricate NPs, laser ablation synthesis in solution (LASiS) generates pure NPs free from any type of contamination and thus, is matchless. In this technique, numerous factors, namely, laser power and wavelength, repetition rate of pulsed laser, spot size of laser beam, and most importantly the medium (solvent) used, etc., control the fabrication of NPs. The medium used for the preparation of NPs in LASiS decides the nature and steadiness of the colloidal NPs that can be further altered/improved by means of varying the pH of the solution. In numerous cases, laser-induced colloidal NPs are extremely reactive as they may react with the media and/or amidst themselves heading for the formation of multifarious configurations and varied agglomerated structures at room temperature provided there exists suitable liquid environment. But one can overcome this agglomeration by the inclusion of certain smart comparable ionic materials that could errand Coulomb repulsion [1], or else the NPs can be enclosed through dissimilar polarity layer that should favor Coulomb repulsion. The tuning of the structure of NPs from core shell to hollow nano structures is also achievable by pH variation. The researchers ought to use metallic nanoparticles for tuning the optical properties of the chosen host or activator (here the lanthanide ions), and for this intention, the sensitivity of NPs is crucial, which predominantly depends on the surface or volume plasmon frequency of NPs along with very negligible involvement of the local field effect. Thus, a deep knowledge and a clear understanding of the comprehensive mechanism of formation of NPs under diverse pH environments is a must. Bismuth-induced nanomaterials encompass exhaustive investigations to become the focal point of further research owing to their new applications (due to its semiconducting properties).

http://dx.doi.org/10.5772/intechopen.70274

The inorganic luminescent rare earth ions and their stable complexes with varied compatible organic ligands enhance the emission of the RE ions in different media. Further, the incorporation of metallic or oxide NPs to the stable RE organic complexes unlocks the prospects for escalating their photoluminescence emission intensity by several orders of magnitude. Numerous researches and deep studies on the improvement of optical properties of RE ions and their complexes in diverse matrices have been approved and are still ongoing [34, 35, 38]. Polyvinyl alcohol (PVA) is a semicrystalline and nontoxic polymer possessing three isomers. Due to the different isomers, it shows a range of absorption and commensurate emission. The emissions are not significant from an application point of view and thus need to be enhanced. The incorporation of NPs comes to rescue and is the one best-suited option. This inclusion of NPs is achievable for the reason that the PVA molecules have large number of voids in their chains. Also, the occurrence of Bi NPs in the PVA molecule can transform/enhance the electronic emission from PVA by means of energy transfer from them and/or their local field effect. The augmentation is realistic for the reason that there exists the buffet of energy level of the PVA molecule as well as the Bi NPs absorbs immensely in the UV region. In the present chapter, differently shaped Bi NPs were prepared by laser ablation in solvents changing the pH of the solvents and characterized by transmission electron microscopy (TEM), SEM, and Raman studies. Laser ablation was used for preparation of Bi NPs in water, sodium hydroxide, and hydrochloric acid. The colloidal solution of as-prepared NPs were separately added to the $Tb^{3+}$ ions and also to $(Tb(Sal)_3(Phen))$ complex in the PVA host polymer to attain thin films. The photoluminescence spectrum of the synthesized polymer films were scrutinized with 266 and 355 nm excitations. The reason for choosing these wavelengths being that the 266 nm excitation wavelength is resonant with the SPR band of Bi NPs, and the 355 radiation for excitation is off-resonant exciting only the Tb ions. Observed augmentation in the photoluminescence emission intensity of the activator terbium ion and its complex in the existence of bismuth NPs entrenched in the PVA host are explained.

## 2. Materials and experiments

All the ingredients terbium oxide, salicylic acid, and 1,10-phenanthroline used were all purchased from Sigma Aldrich. $Tb_4O_7$ and Sal were 99.9% pure. 1,10-phenanthroline was 99.5% pure. Bismuth plate with purity 99.0% was obtained from the same company and used for ablation and preparation of NPs.

### 2.1. Laser ablation technique to prepare Bi NPs

Laser ablation technique was used to prepare Bi NPs at different pH in different aqueous solutions (namely, water (H), water + sodium hydroxide (HN), and water + hydrochloric acid (HC)). **Figure 4** shows the experimental set up used for laser ablation for the production of Bi nanoparticles.

The irradiation source was the different wavelengths of an Nd:YAG laser with 7 ns pulse duration. The laser beam was tightly focused with the help of a short focal length (10 cm focal

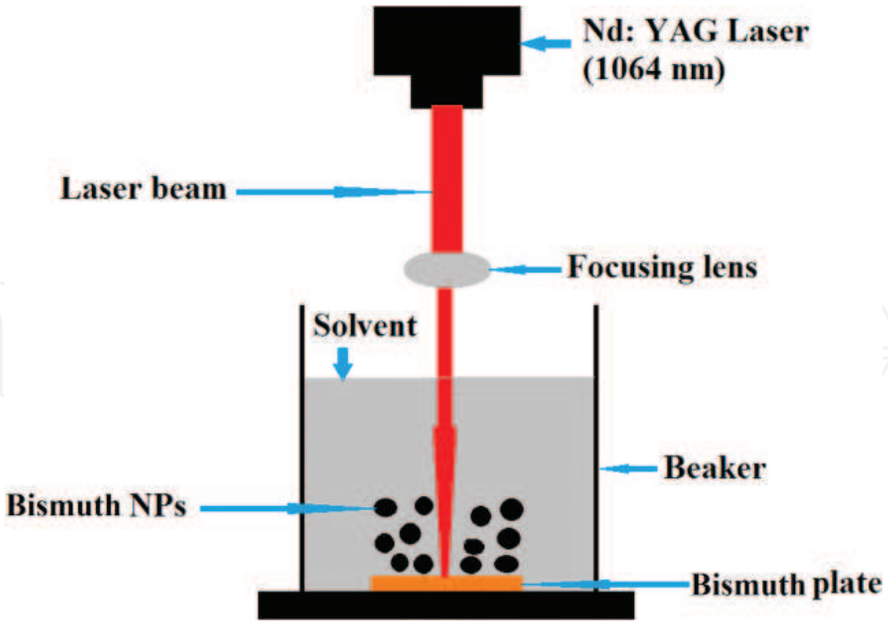


**Figure 4.** Experimental setup of laser ablation for preparation of Bi nanoparticles.

length) convergent lens on the copper plate (thickness: 0.6 mm, size: 18 × 30 $mm^2$) kept in a beaker with water 2.5 mm deep from the top surface. The liquid was continuously stirred using a magnetic stirrer. Laser ablation was continued for 45 min. The Bi plate was taken out of the liquid, and the sample was used for optical measurements and preparation of thin film samples. The same procedure was repeated for water + sodium hydroxide (HN), and water + hydrochloric acid.

### 2.2. Preparation of $Tb(Sal)_3(Phen)$ complex

0.010 mmol $Tb_4O_7$ was obtained by dissolving $Tb_4O_7$ in hydrochloric acid to obtain $TbCl_3$ solution. 0.015 mmol of salicylic acid and 0.005 mmol 1,10-phenanthroline were independently dissolved in 2.0 ml ethanol to get its ethanolic solution. Both were added and stirred rigorously for an hour to achieve $Tb(Sal)_3(Phen)$ complex as explained by Kaur et al. [21].

### 2.3. Preparation of polymer film with $Tb^{3+}$ complex and Bi nanoparticles

Polyvinyl alcohol was dissolved in double distilled water to attain its 0.011 mmol transparent homogeneous solution. From the already-prepared laser ablated Bi nanoparticles in water, 5 ml of colloidal NPs were mixed separately with ethanolic solution of the as-prepared $Tb(Sal)_3(Phen)$ complex. The mixture was homogenized using a magnetic stirrer for 2 hours at room temperature and dispensed in aqueous solution of PVA. The resulting mixture was stirred thoroughly for 4–5 h and later poured in the polypropylene Petri dish and allowed to dry at its own without any heating agent to obtain the thin films. Flowchart depicting the steps for the preparation of polymer samples is shown in **Figure 5**.

http://dx.doi.org/10.5772/intechopen.70274

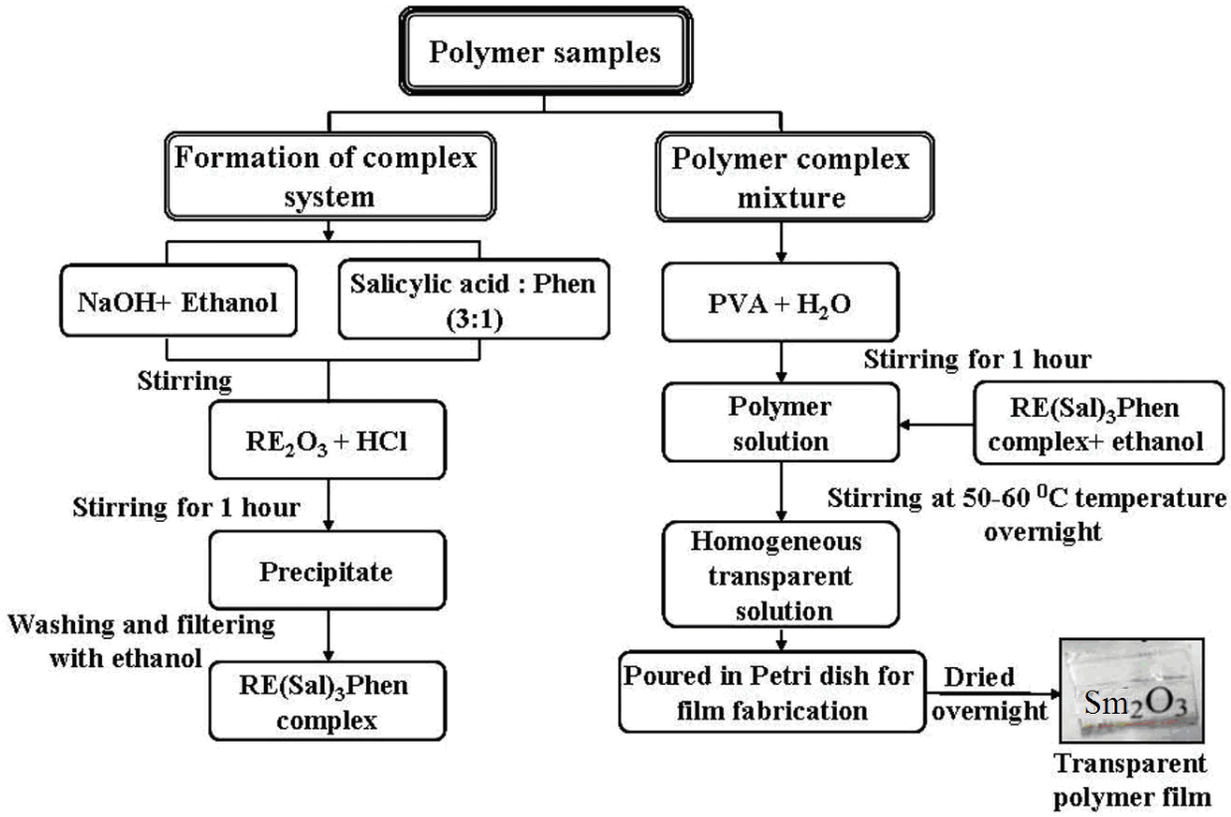


**Figure 5.** Flowchart depicting the steps for the preparation of polymer samples.

## 3. Results and discussions

### 3.1. Structural analysis using transmission electron microscopy (TEM)

TEM micrograph of Bi NPs in water, i.e., H (pH = 7) is shown in **Figure 6(a)**. The particles with average particle size of 14 nm and spherical in nature are observed. **Figure 6(b)** shows the size distribution of the particles as a histogram. The nanoparticles are poly-crystalline as seen from their selected area electron diffraction (SAED) patterns as shown in **Figure 6(c)**. Later, we supplemented it with significant amounts of acid and base to water separately to examine the consequence of pH on the size/dimension, contour/shape, and arrangement of NPs. At pH 9.7, namely, the medium is basic now, one monitors agglomerated core shell type NPs that are depicted in **Figure 6(d)**. An enlarged vision of core shell NPs is shown in its inset, verifying core diameter ~8 nm and shell thickness ~6 nm for the core shell NPs. **Figure 6(e)** demonstrates the histogram for its size distribution and the average size of NPs was found to be 18 nm. The SAED pattern for the same is given in **Figure 6(e)**. Here, the agglomeration of nanoparticles exists that leads to formation of bigger nanoparticles. This is due to the occurrence of the opposite polarity ($Na^+$ and $OH^-$) on the different NPs.

Spherical nanoparticles are formed when the pH of the sample is 7 (i.e., NPs prepared in pure water). Interestingly, when we add HCl in water and make the pH of the solution to 2.3,

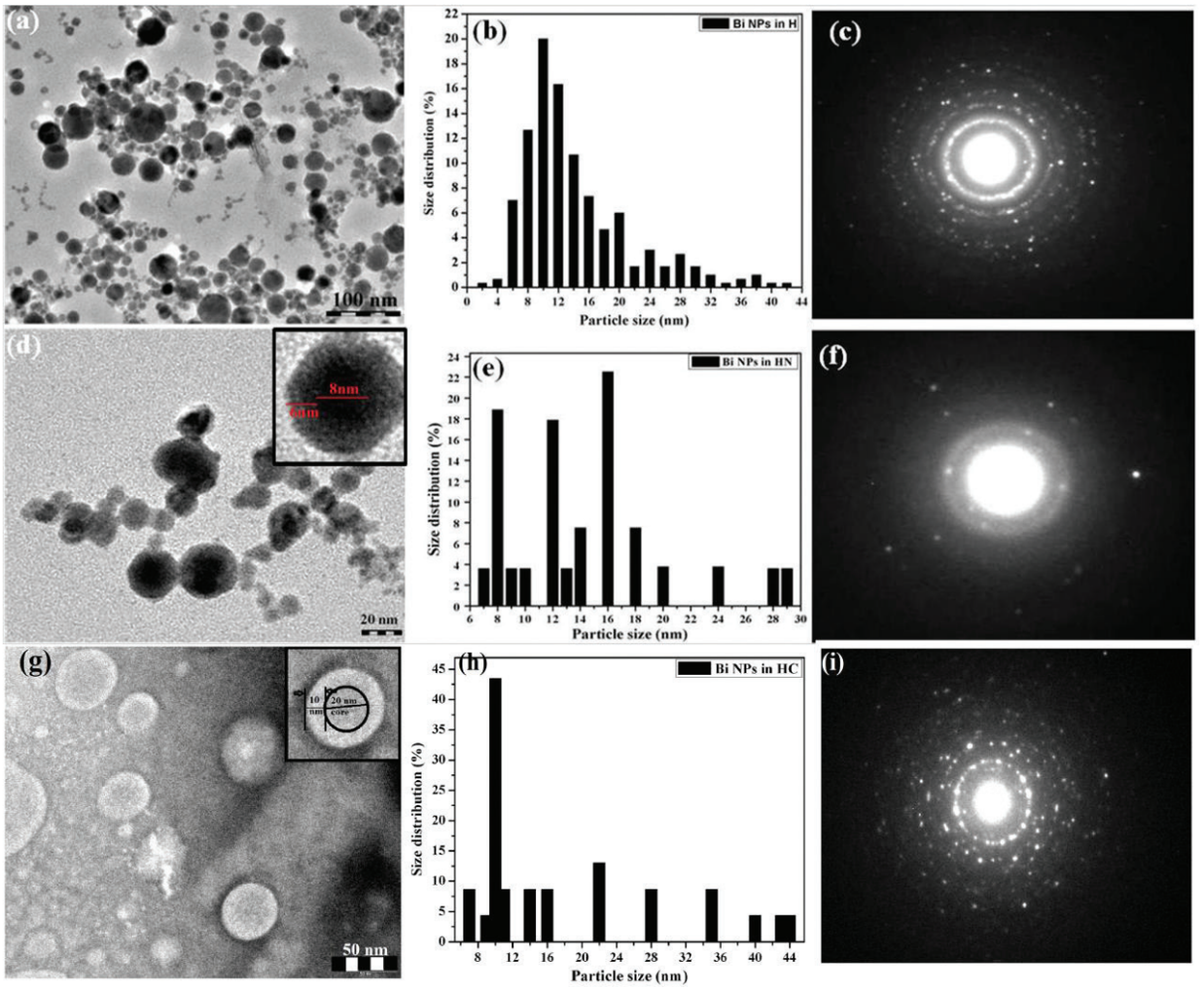


**Figure 6.** (a–c) TEM images of Bi NPs, particle size distribution, and SAED pattern in aqueous solution of H. (d–f) TEM images of Bi NPs, particle size distribution and SAED pattern in aqueous solution of HN. Inset of figure in (d) shows formation of core shell NPs. (g–i) TEM images of Bi NPs aqueous solution in water + HC with enlarged view of NPs with core size in the inset, particle size distribution and its SAED pattern (reproduced from Kumar et al. [48]).

the prepared NPs appear as hollow core shell NPs as shown in the TEM micrograph in **Figure 6(f)**. The average size of the NPs ranges between 15 and 45 nm (see **Figure 6(g)**). A few particles are bigger as they have swollen up. The diameter of the hollow core and thickness of shell is measured to be 20 and 10 nm, respectively, as shown in the inset of **Figure 6(g)**. **Figure 6(h)** shows the size distribution of the particles with average size of 21 nm. The SAED pattern presenting polycrystalline character is revealed in **Figure 6(i)**. All annotations provide evident confirmation that the shape of NPs depends on the pH of the used medium. The character of NPs transforms to hollow from core shell if we alter the pH and change it to acidic from the basic one.

The formation of hollow NPs can be understood on the basis of the Kirkendall effect [25]. The creation of bismuth nano particles initiate as soon as the laser beam is incident on the metallic plate of bismuth and focused carefully. Now the pH of the medium plays a crucial role. Spherical Bi NPs are formed in neutral pH. But the case differs for the acidic medium,

http://dx.doi.org/10.5772/intechopen.70274

as a few of the formed bismuth NPs react with the medium to produce bismuth oxychloride (BiOCl) that gets coated on the bismuth core NPs with the passage of time of ablation. It is noteworthy that the diffusion of bismuth ions is exceedingly rapid when compared to that of chloride ions. The difference in the diffusion rate generates vacancies in the core of bismuth NPs, and when these vacancies are formed in surplus, these join together to form voids. Because of these analogous reasons and facts, core-shell configuration is commonly observed to form voids in larger NPs. Even the created voids are not proportional in every case. This is probably owing to formation of partial hollow nanospheres as observed in CdS/Cd hollow NPs by researchers [5].

One does not observe the formation of hollow NPs when pH of media changes to basic. The reason accounted for this is possibly that in this case, bismuth hydroxide forms the shell and gets deposited on the bismuth core. Here in this case, the diffusivity of hydroxide ion is greatly better than that of bismuth ion. Consequently, there is a superior possibility of formation of vacancies in the core to acquire a core-shell type structure. This, moreover, augments the density of particles in the core and diminishes their amount in the shell.

### 3.2. Structural study using scanning electron microscopy (SEM)

Bi NPs in aqueous solution of H, HN, and HC, respectively, were added to the polymer films and their SEM images are shown in **Figure 7**(**a–c**). The nanoparticles appear embedded in the case of water and basic medium, but in acidic media, some of the bismuth NPs reacts with acid to form flower-like clusters of BiOCl that are quite obvious in **Figure 7(c)**.

### 3.3. Raman measurement

To understand the formation of Bi NPs and their compounds attributed to different environments (H, HN, and HC), the Raman spectra of colloidal Bi NPs were measured. Raman spectrum of Bi NPs in aqueous solution of water (H), water + NaOH (HN), and water + HCl (HC),

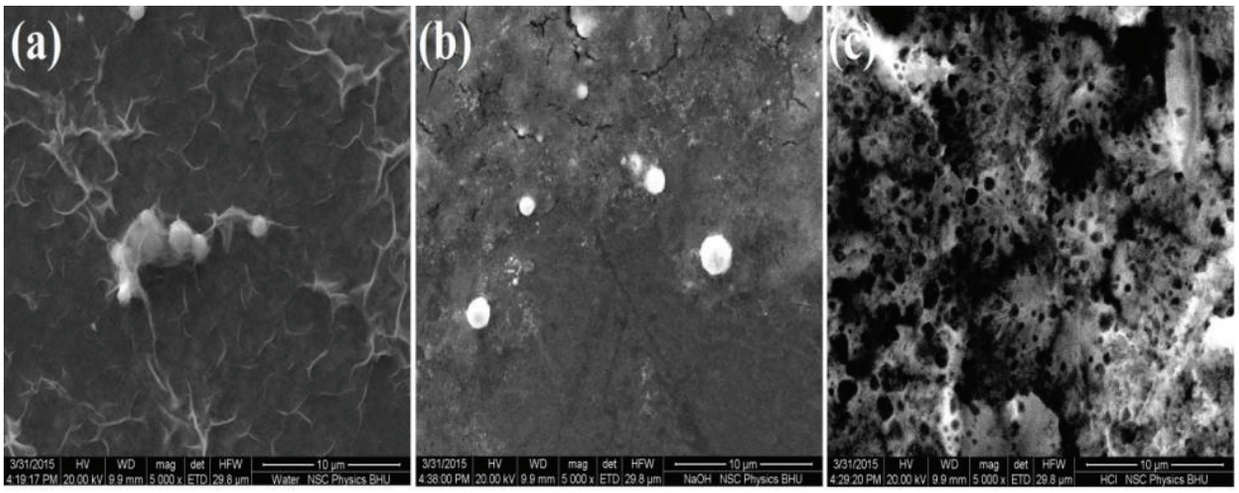


**Figure 7.** SEM images of Bi NPs in polymer films with H (a), HN (b) and HC (c) respectively (reproduced from Kumar et al. [48]).

respectively, in the range 50–400 $cm^{-1}$ are depicted in **Figure 8(a)–(c)**. The spectra demonstrate numerous active vibrational modes in this frequency range. These bands are customized by the environment and bestow lucid information about molecules formed in different media.

**Figure 8(a)** shows the Raman vibrational peaks owing to Bi NPs in water. Two vibrational bands at 66.48 and 92.51 $cm^{-1}$ are observed that can be attributed to pure Bi NPs in the host [11, 18, 30, 31]. Both these peaks depend upon the particle size. The former lower frequency band is assigned to the $E_g$ mode and the later corresponds to $A_{1g}$ mode. Generally, the vibrational frequencies of $A_{1g}$ mode of Bi NPs lie between 85 and 95 $cm^{-1}$, and the Raman frequencies of the lower $E_g$ mode lie between 59 and 75 $cm^{-1}$, which get somewhat modified with the size of the nanoparticles and transfer toward lower frequencies for smaller nanoparticles.

But the case is very different on changing the pH of the medium by adding NaOH (HN). **Figure 8(b)** depicts the Raman vibrational peaks of Bi NPs in HN. The peaks for the $E_g$ and $A_{1g}$ modes in the basic medium shift to 65.25 and 92.73 $cm^{-1}$ with full width at half maxima 9.86 and 10.51 $cm^{-1}$, respectively. Two other peaks also emerge at 121.82 and 312.56 $cm^{-1}$ in the spectrum. These Raman bands are assigned to Bi—O stretching vibrations confirming that the species formed as nanoparticles are due to $\alpha$-$Bi_2O_3$ [8, 15]. Similarly, by decreasing the pH of the medium on the addition of considerable quantity of HCl to make it acidic, namely HC, the intensity of the Raman bands gets reduced when compared with the bands of Bi NPs in H and HN (see **Figure 8(c)**). In this case, an intense peak is seen at 141.24 $cm^{-1}$ along with weak

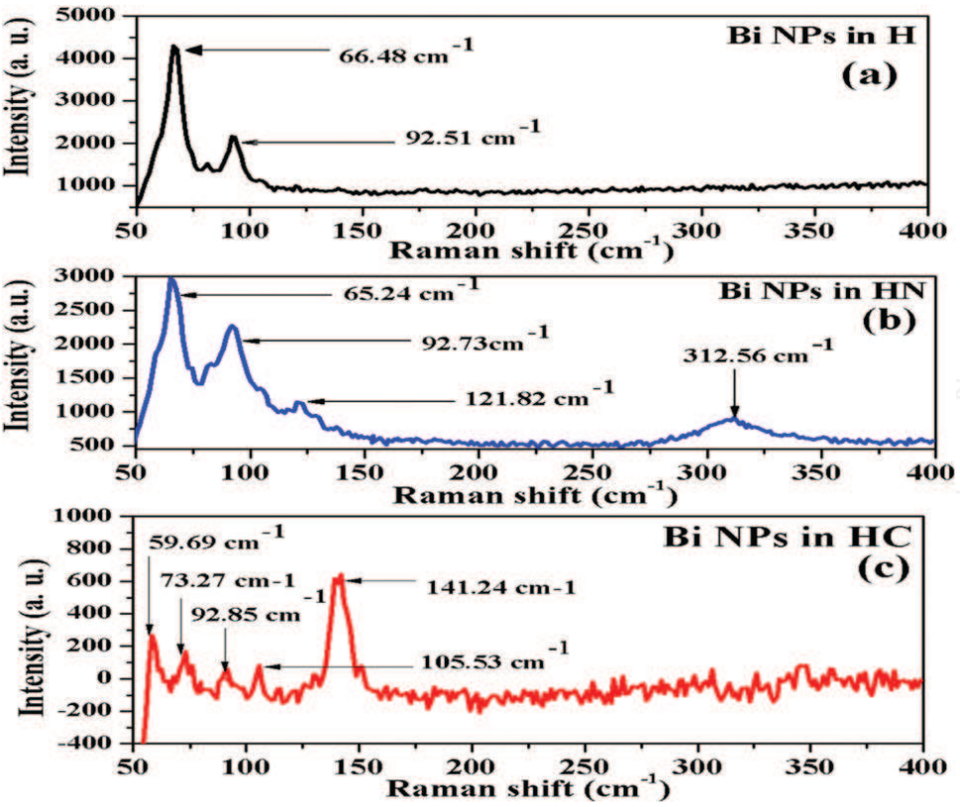


**Figure 8.** (a–c) Raman spectrum of Bi NPs in aqueous solution of water (H), water + NaOH (HN), and water + HCl (HC), respectively (reproduced from Kumar et al. [48]).

http://dx.doi.org/10.5772/intechopen.70274

bands observed at 59.69, 73.27, 92.85, and 105.53 $cm^{-1}$. The weaker Raman bands are assigned to the $E_g$ and $A_{1g}$ modes of vibration for Bi in $\alpha$-$Bi_2O_3$. The band observed at 105.53 $cm^{-1}$ may be attributed to Bi for $\alpha$-$Bi_2O_3$ phase [12, 32]. The two peaks observed in HN at 121.82 and 312.56 $cm^{-1}$ disappear here. This shows that the vibrational modes of Bi in $\alpha$-$Bi_2O_3$ dominate over Bi—O vibration in $\alpha$-$Bi_2O_3$. In this case (i.e., HC), two new Raman peaks are observed at 141.24 (stronger) and 59.69 $cm^{-1}$ (weaker) due to BiOCl molecule [45, 47]. The former peak is attributed to internal stretching of Bi—Cl, and the later weaker one is assigned to its external stretching [39–41]. A weak band appears at 396 $cm^{-1}$, which is a consequence of the motion of the oxygen atom and designated as $B_{1g}$ band, but it is not optically considerable in this case. It is necessary to mention that in the laser ablation synthesis in solution, momentous chemical processes occur after the ablation of the target. Consequently, the intensity of the peaks is correlated to the concentration of a particular species developed at that instant. Thus, one may infer that the intense band at 141.24 $cm^{-1}$ due to BiOCl evidently suggests its larger concentration. The positions of the Raman peaks for Bi NPs in H, HN, and HC along with their full width at half maxima (FWHM) and their respective intensity are tabulated in **Table 1**.

### 3.4. UV-Vis absorption

**Figure 9** shows the absorption spectra of Bi NPs in H, HN, and HC solutions. The absorption peak for Bi NPs in water emerges at 265 nm. This is accredited to the plasmonic peak frequency of Bi NPs. In the case of HN, two peaks are observed. The first peak at 233 nm is attributed to the plasmon frequency of $Bi_2O_3$ and the second peak at 274 nm is associated with that of Bi NPs. There is a shift in the Bi plasmon peak toward higher wavelength in this case as compared to the Bi plasmon peak in pure water (265 nm) that supports the agglomeration of Bi NPs. Absorption

| | | | | | | |
|---|---|---|---|---|---|---|
| Bi NPs in H | Raman peak position ($cm^{-1}$) | 66.48 | 92.51 | — | — | — |
| | FWHM ($cm^{-1}$) | 7.49 | 5.78 | — | — | — |
| | Normalized intensity | 0.99 | 0.44 | — | — | — |
| Bi NPs in HN | Raman peak position ($cm^{-1}$) | 65.25 | 92.73 | 121.82 | 312.56 | — |
| | FWHM ($cm^{-1}$) | 9.86 | 10.51 | 3.71 | 33.06 | — |
| | Normalized intensity | 0.98 | 0.71 | 0.26 | 0.17 | — |
| Bi NPs in HC | Raman peak position ($cm^{-1}$) | 59.69 | 73.26 | 92.85 | 105.53 | 141.24 |
| | FWHW ($cm^{-1}$) | 2.86 | 4.89 | 4.04 | 2.71 | 9.01 |
| | Normalized intensity | 0.80 | 0.74 | 0.69 | 0.70 | 0.98 |

**Table 1.** Raman peaks position, FWHM, and normalized intensity of Bi NPs in water (H), water + NaOH (HN), and water + HCL (HC).

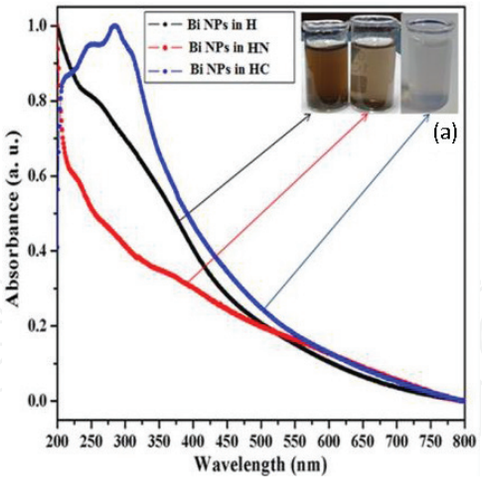


**Figure 9.** UV-Vis-NIR absorption spectrum of Bi NPs in aqueous solution of H, HN, and HC and inset figure shows their corresponding color (a) (reproduced from Kumar et al. [48]).

spectra for Bi NPs in HC sample show a weird behavior with absorption peaks at 245, 285, and 309 nm that are attributed to $Bi_2O_3$, Bi NPs, and BiOCl. The main plasmon peak is shifted slightly further toward higher wavelengths. The shifting of the absorption peak to the higher wavelength region is an indication of increased agglomeration of NPs. Wang et al. [41] have reported the absorption peak at 267 nm due to semimetal bismuth NPs in PVP solution. Creighton and Desmond [6] have reported the absorption band around 270–280 nm for bismuth particles of size ranging in 10 nm. This inconsistency in intensity of the absorption peaks appears as an outcome of the concentration of the species in solution. The inset to **Figure 9** shows the color of the colloidal solution after ablation. Different colors signify formation of Bi NPs and their conversion to additional forms, namely $Bi_2O_3$, BiOCl, or Bi NPs and its core shell structure.

The surface Plasmon resonance is the characteristic of NPs embedded in a dielectric host and is ascribed to combined oscillations of the electrons responding to the optical excitation energy. Optical absorption spectrum of Bi NPs prepared in water by laser ablation for 20 min is shown in **Figure 10**, which depicts its characteristic surface plasmon resonance peak at 267 nm together with a diminutive band at 283 nm that may be assigned to $^4S_{3/2} \rightarrow {}^2P_{3/2}$ of $Bi^0$ transitions [33]. On ablation of the bismuth target for 40 min, the peak at 267 nm is observed to diminish, and the intensity of the peak at 283 nm started increasing, which indicates that the $Bi^{3+}$ ions are reduced completely to bismuth NPs [9, 17, 40, 41] Also, it is observed that the NPs get agglomerated giving bigger-sized NPs on ablation for a longer period and, hence, absorption at a longer wavelength. Gutierrez and Henglein [14] reported that nanometer-sized bismuth particles exhibited an absorption at ~253 nm, and according to Creighton and Desmond [6], the first absorption band of 10 nm bismuth particles should appear around 270–280 nm. Polyvinylpyrroldone-stabilized bismuth NPs have been synthesized by Wang et al. [41] with an absorption peak at 281 nm. Our result fits well with the above two literature values.

The absorption spectrum of $(Tb(Sal)_3(Phen))$ complex in PVA with and without laser-ablated Bi NPs are also shown in **Figure 10**. The $(Tb(Sal)_3(Phen))$ complex in the PVA film shows a band centered at 315 nm that may be attributed to the $S_0 \rightarrow S_1$ singlet state absorption of salicylic acid. Also, the absorption band due to $\pi \rightarrow \pi^*$ transition of PVA exists in this region, so

http://dx.doi.org/10.5772/intechopen.70274

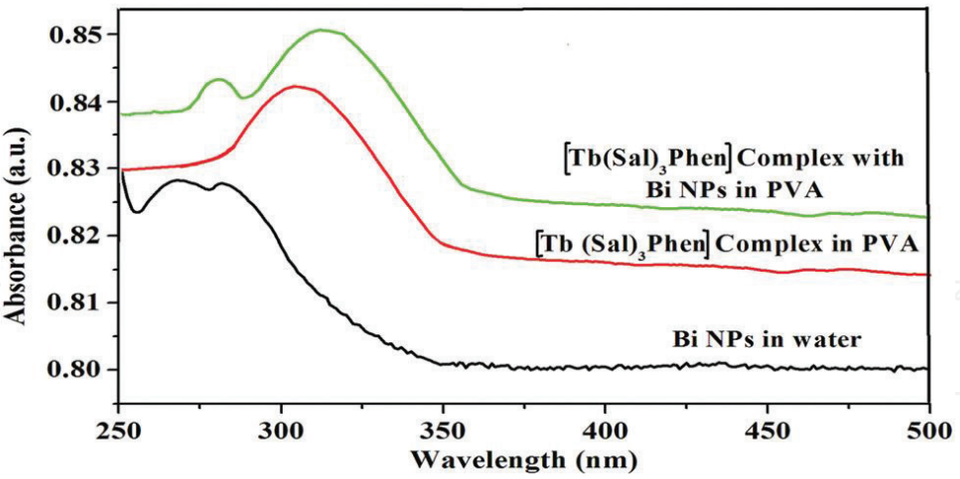


**Figure 10.** Absorption spectra of Bi NPs in water ablated for 20 min, $(Tb(Sal)_3(Phen))$ complex in PVA and $(Tb(Sal)_3(Phen))$ complex with Bi NPs in PVA (reproduced from Kaur et al. [24]).

there may be an overlapping of the absorption bands of PVA and Sal. The $(Tb(Sal)_3(Phen))$ complex with Bi NPs in PVA illustrates an absorption peak for Bi NPs along with the absorption band of Sal. It is observed that this band of Sal shows a red shift of ~8 nm on addition of Bi NPs along with the $(Tb(Sal)_3(Phen))$ complex in PVA film. The shift can be ascribed to aggregation of the complex through NPs.

## 4. Excitation spectra

The photoluminescence excitation spectra of $Tb^{3+}$ ions in PVA, $Tb^{3+}$ ions with Bi NPs in PVA and $(Tb(Sal)_3(Phen))$ complex with Bi NPs in PVA corresponding to the $^5D_4 \rightarrow {}^7F_5$ transition of $Tb^{3+}$ ion monitored at 544 nm were recorded and are shown in **Figure 11**.

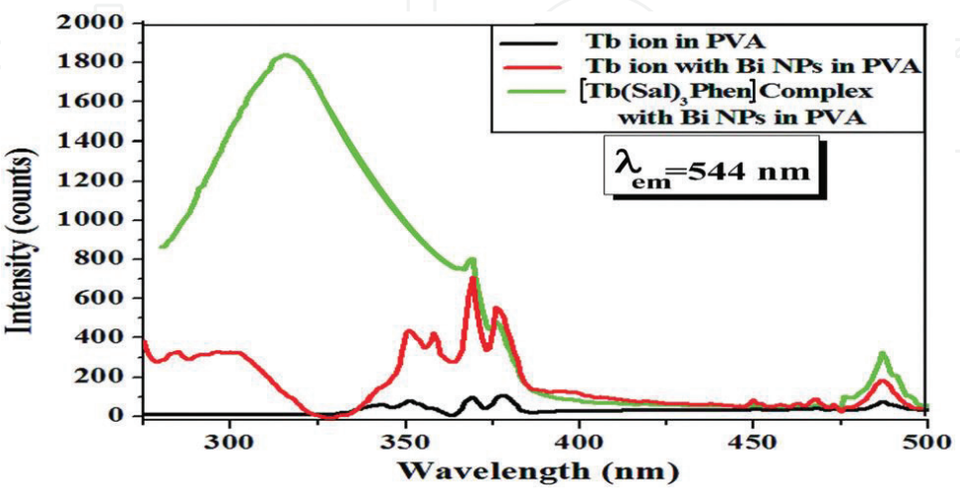


**Figure 11.** Excitation spectra of $Tb^{3+}$ ions in PVA, $Tb^{3+}$ ions with Bi NPs in PVA and the $(Tb(Sal)_3(Phen))$ complex with Bi NPs in PVA corresponding to the $^5D_4 \rightarrow {}^7F_5$ transition of $Tb^{3+}$ ions monitored at 544 nm (reproduced from Kaur et al. [24]).

The excitation spectrum of $Tb^{3+}$ ion in PVA sample also shows a few weak bands at 341, 352, 358, 369, 377, and 488 nm wavelengths corresponding to absorption of $Tb^{3+}$ ions. When Bi NPs were added to $TbCl_3$, the excitation intensity of the bands got improved. There also appears a weak broad plasmonic band for Bi NPs at 285 nm. The excitation spectrum ($Tb(Sal)_3(Phen)$) complex and laser-ablated Bi NPs in PVA depicts an extensive excitation band between 275 and 375 nm that may be attributed to $n \rightarrow \pi^*$ transition of the salicylate ligands. There seems to be appreciable enhancement in the intensity of the bands corresponding to the $Tb^{3+}$ ion emission. This vividly signifies effectual sensitization of $Tb^{3+}$ ions by the ligands pointing to a competent antenna effect [20].

## 5. Photoluminescence using 266 nm wavelength

The photoluminescence spectra depicts the emission bands of $Tb^{3+}$ ions, $Tb^{3+}$ ions with Bi NPs and the ($Tb(Sal)_3(Phen)$) complex with Bi NPs in PVA in the range of 375–700 nm on excitation with the SPR band of NPs using 266 nm radiation and is shown in **Figure 12**.

The spectra of $Tb^{3+}$ ions exhibit characteristic emission peaks at 487, 544, 583, and 618 nm for $Tb^{3+}$ ions emanating from $^5D_4 \rightarrow {}^7F_J$ (J = 6, 5, 4, 3) transitions, respectively, and among them, the $^5D_4 \rightarrow {}^7F_5$ transition (544 nm) is the most intense one. The emission intensity of $Tb^{3+}$ bands was enhanced on incorporating Bi NPs, but the effect is more prominent in the case of the ($Tb(Sal)_3(Phen)$) complex in PVA as in this case, the emission emanating from the $^5D_3$ level also appear, which is an additional interesting feature.

The mechanism for augmentation of the emission intensity of the observed transitions may be elucidated with the help of a partial energy-level diagram showing different routes of excitation of $Tb^{3+}$ ions, and the respective emissions are shown in **Figure 13**. Primarily, the 266 nm photon excites the $^5H_7$ level through the $^7F_6 \rightarrow {}^5H_7$ absorption transition of $Tb^{3+}$ ions. Then the excited $Tb^{3+}$ ions relax nonradiatively down to $^5D_3$ and $^5D_4$ levels to yield the emissions from these level to lower lying levels ($^7F_J$; J = 1–6). This excitation radiation, i.e., 266 nm, moreover,

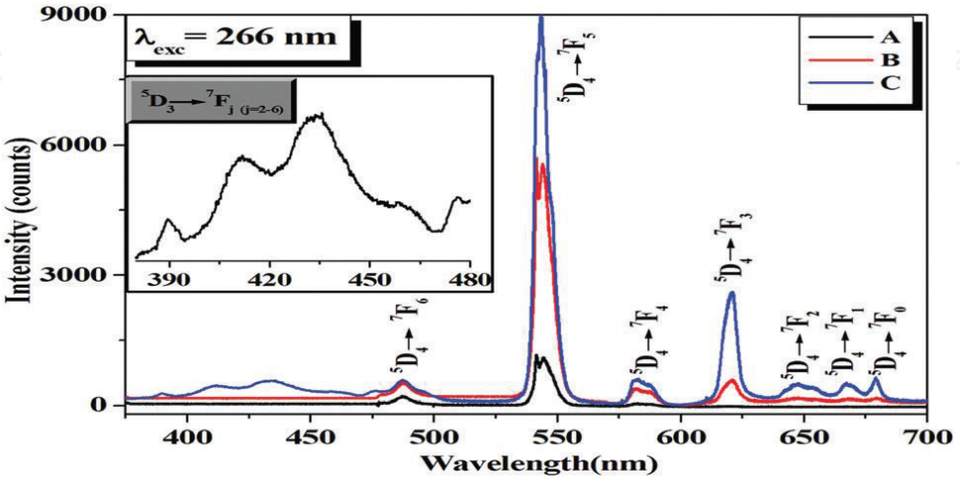


**Figure 12.** Photoluminescence spectra of $Tb^{3+}$ ions (A), $Tb^{3+}$ ions with Bi nanoparticles (B) and the ($Tb(Sal)_3(Phen)$) complex with Bi NPs (C) in PVA in the range of 375–700 nm using 266 nm radiation exciting the SPR band of Bi NPs (reproduced from Kaur et al. [24]).

http://dx.doi.org/10.5772/intechopen.70274

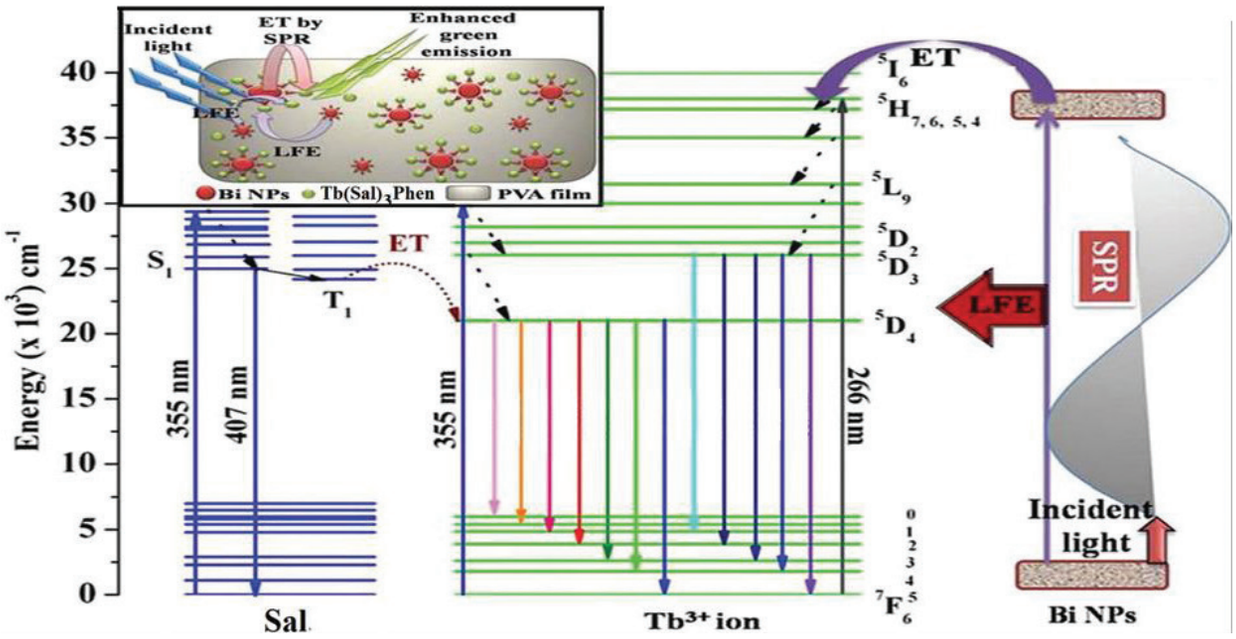


**Figure 13.** Partial energy-level diagram showing different routes of excitation of $Tb^{3+}$ ions and the respective emissions exciting the SPR band of Bi NPs and the Sal ligand, respectively, on excitation with 266 and 355 nm radiations for improved green emission. The inset to the figure depicts $Tb^{3+}$ ions, Bi NPs, and ($Tb(Sal)_3(Phen)$) complex in PVA host presenting the plasmonic and the field effect to boost the emission of $Tb^{3+}$ ion. SPR refers to surface plasmon resonance, LFE stands for local field effect, and ET represents energy transfer (reproduced from Kaur et al. [24]).

excites the surface plasmon band of Bi NPs. This engrossed excitation energy from the surface plasmon band of Bi NPs is transferred to $Tb^{3+}$ ions. It further improves the build up of population of higher $^5D_3$ and $^5D_4$ levels of $Tb^{3+}$ ion. This is cause for enhancement in the photoluminescence emission intensity. The great absorption cross-section of the bismuth plasmon band grounds for an amplified excitation of $^5D_4$ level of $Tb^{3+}$ ion by means of energy transfer from the excited surface plasmon resonance band of Bi NPs. It is noteworthy to mention that the ligand Sal does not absorb at 266 nm radiation as no energy level of Sal exists at this energy. It merely encapsulates the $Tb^{3+}$ ion to cut it off from the host vibrations and intensifies the emission from the complexed $Tb^{3+}$ ion, thus resulting in the emergence of emission from the $^5D_3$ level.

## 6. Photoluminescence using 355 nm wavelength

The photoluminescence spectra of $Tb^{3+}$ ion, $Tb^{3+}$ ion with Bi NPs and ($Tb(Sal)_3(Phen)$) complex with Bi NPs in PVA in the range between 375 and 700 nm using 355 nm excitation radiation, namely, nonresonant excitation is shown in **Figure 14**. The photoluminescence emission spectra is similar to the previous one, but the photoluminescence emission intensity for ($Tb(Sal)_3(Phen)$) complex with Bi NPs is enhanced to a large extent in the present case. This improvement in the photoluminescence emission intensity can be understood by the following mechanism.

This nonresonant 355 nm excitation radiation excites equally the $Tb^{3+}$ ion in addition to the Sal ligand to their excited states. It should be mentioned here that the Bi NPs do not absorb this wavelength. This incident excitation energy is directly absorbed by the $^5L_9$ level of $Tb^{3+}$ ion. It

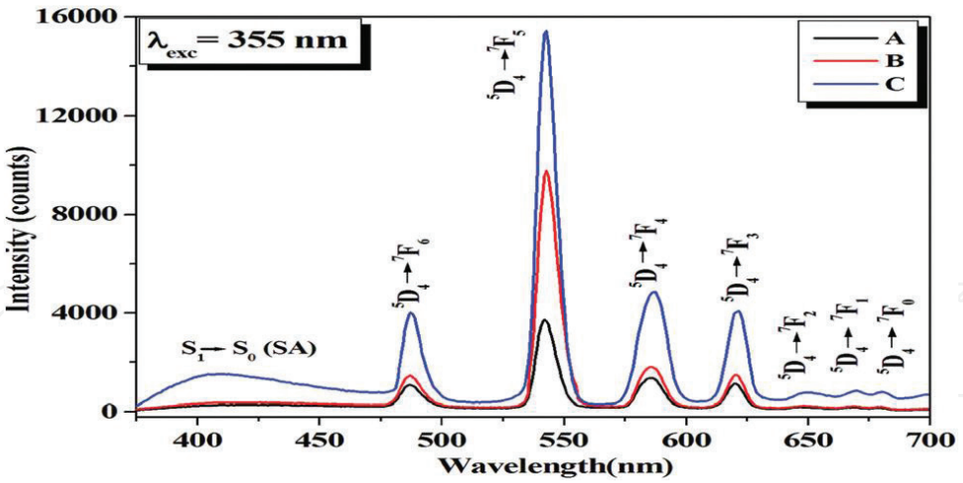


**Figure 14.** Photoluminescence spectra of $Tb^{3+}$ ions (A), $Tb^{3+}$ ions with Bi NPs (B), and $(Tb(Sal)_3(Phen))$ complex with Bi NPs (C) in PVA in the range of 375–700 nm on excitation with 355 nm radiation (reproduced from Kaur et al. [24]).

then relaxes nonradiatively and populates the emitting $^5D_4$ level. Along with this, the optical energy absorbed by the Sal ligand is also transferred to the resonating $Tb^{3+}$ ions populating the $^5D_4$ level via intersystem crossing and the consequent energy transfer process that is the reason for enhancing the emission intensity. Also, the Bi NPs form a local plasmonic field around the $(Tb(Sal)_3(Phen))$ complex, and the high-field gradients of NPs increase the lifetime of the emitting $^5D_4$ level of $Tb^{3+}$ ions [42]. The coupling between the radiative transitions, and the field effect is the fundamental basis for the enhancement in intensity as shown in the inset of **Figure 14**. The increase in the lifetime of the $^5D_4$ level of $Tb^{3+}$ ion is clearly observed in the decay curves for the $^5D_4 \rightarrow {}^7F_5$ transition of $Tb^{3+}$ ions in the presence and absence of Bi NPs (as seen in **Figure 15**). Herein, the point to mention is that different transitions of $Tb^{3+}$ ion respond differently to the

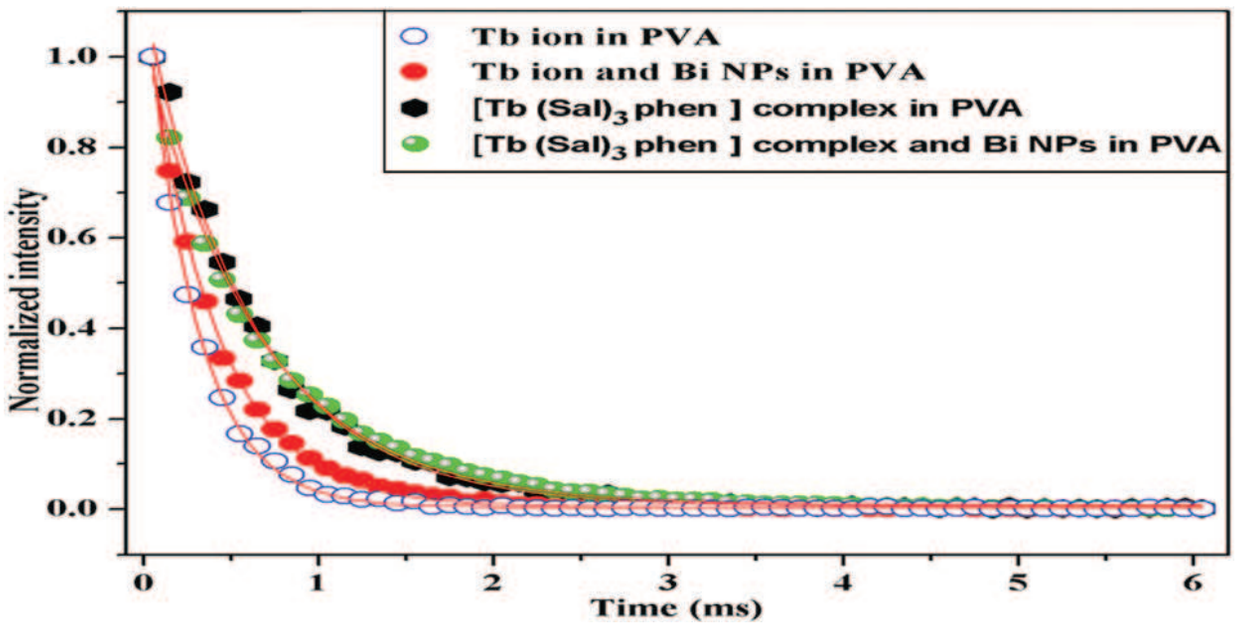


**Figure 15.** The decay curves for the $^5D_4 \rightarrow {}^7F_5$ transition at 544 nm of $Tb^{3+}$ ions with and without NPs and the $(Tb(Sal)_3(Phen))$ complex with and without Bi NPs in PVA using 355 nm radiation (reproduced from Kaur et al. [24].

http://dx.doi.org/10.5772/intechopen.70274

local field gradients of Bi NPs. The reason behind this may be that magnetically allowed dipole transitions differ in interaction with the surface plasmon field of NPs than the electrically allowed dipole transitions. Nevertheless, the photoluminescence emission intensity of $Tb^{3+}$ ion on excitation with 355 nm nonresonant radiation is larger to a great extent than that of 266 nm resonant excitation. It undoubtedly reveals that the transfer of energy to $Tb^{3+}$ ions through the salicylic acid ligand is more proficient as compared with other channels of energy transfer.

## 7. Time-resolved photoluminescence spectroscopy

**Figure 15** represents the decay curves for the $^5D_4 \rightarrow {}^7F_5$ transition monitored at 544 nm of $Tb^{3+}$ ions with and without Bi NPs and the $(Tb(Sal)_3(Phen))$ complex with Bi NPs in PVA using 355 nm radiation.

The decay curves were fitted with first-order exponential fits that lead to a larger lifetime of $^5D_4$ level of $Tb^{3+}$ ions in the presence of NPs. The values obtained for lifetimes are tabulated in **Table 2**.

This increase in lifetime is explained due to the local surface fields of Bi NPs as given in the inset of **Figure 13**. Thus, photoluminescence properties of polymer-doped RE complexes can be improved by adding NPs [22]. There is a substantial improvement in the lifetime values when Bi NPs are added to the $TbCl_3$ in PVA and, alternatively, for the $(Tb(Sal)_3(Phen))$ complex, there is just a small increase in the lifetime.

| Sample | Lifetime (μs) |
|---|---|
| $Tb^{3+}$ ions in PVA | 287 |
| $Tb^{3+}$ ions with Bi NPs in PVA | 399 |
| $(Tb(Sal)_3(Phen))$ in PVA | 625 |
| $(Tb(Sal)_3(Phen))$ with Bi NPs in PVA | 659 |

**Table 2.** The values for the lifetime of $Tb^{3+}$ ions, $Tb^{3+}$ ions with Bi NPs, $(Tb(Sal)_3(Phen))$ complex with Bi NPs, and $(Tb(Sal)_3(Phen))$ with Bi NPs in PVA.

## 8. Conclusion

To recapitulate, bismuth nanoparticles have been prepared by laser ablation technique at in different aqueous solutions, namely water, water + sodium hydroxide, and water + hydrochloric acid. TEM micrographs confirm the formation of spherical, core shell, and hollow spheres in H, HN, and HC, respectively, with variation in size. Further, the Bi NPs were subsequently scattered with $Tb^{3+}$ ions and their complex with salicylic acid (Sal) and 1,10-phenanthroline in aqueous solution of polyvinyl alcohol to get thin polymer films. Then the photoluminescence properties of $Tb^{3+}$ ions and the $(Tb(Sal)_3(Phen))$ complex were studied using 266 and 355 nm

as excitation wavelengths. The emission efficiency of $Tb^{3+}$ ions and their complex is seen to be enhanced in the presence of Bi NPs on excitation with both the radiations. On 266 nm excitation, a comprehensive photoluminescence emission spectrum of $Tb^{3+}$ ions is observed for $Tb(Sal)_3(Phen)$ complex with Bi NPs spanning the region between 375 and 700 nm depicting transitions from $^5D_3/^5D_4$ levels to diverse $^7F_J$ levels. It is worthy to mention that the luminescence enhancement is better for ($Tb(Sal)_3(Phen)$) complex with 355 nm excitation radiation. The augmentation in intensity is ascribed to the coupling of plasmonic and local field effect of Bi nanoparticles on $Tb^{3+}$ ion that influence the lifetime of radiative level of $Tb^{3+}$ ion in addition to transfer of energy from Sal to $Tb^{3+}$ ion.

## Acknowledgements

G. Kaur acknowledges DST for the project grant in the form of SR/WOS-A/PS-57/2013 and RSC advances and Dalton Transactions for the reproduction of figures.

## Author details

Gagandeep Kaur*, Brijesh Kumar and S.B. Rai

*Address all correspondence to: gagandeep_bhu@yahoo.com

Laser and Spectroscopy Laboratory, Department of Physics, Banaras Hindu University, Varanasi, India

## References

[1] Amendola V, Meneghetti M. Laser ablation synthesis in solution and size manipulation of noble metal nanoparticles. Physical Chemistry Chemical Physics. 2009;**11**:3805-3821

[2] Balan L, Schneider R, Billaud D, Fort Y, Ghanbaja J. A new synthesis of ultrafine nanometre-sized bismuth particles. Nanotechnology. 2004;**15**:940-944

[3] Binnemans K. Lanthanide-based luminescent hybrid materials. Chemical Reviews. 2009; **109**;4283-4374

[4] Bekiari V, Lianos P. Multicolor emission from terpyridine lanthanide ion complexes encapsulated in nanocomposite silica/poly (ethyleneglycol) sol–gel matrices. Journal of Luminescence. 2003;**101**:135-140

[5] Cabot A, Smith RK, Yin Y, Zheng H, Reinhard BM, Liu H, Alivisatos AP. Sulfidation of cadmium at the nanoscale. ACS Nano. 2008;**2**:1452-1458

[6] Creighton JA, Desmond GE. Ultraviolet-visible absorption spectra of the colloidal metallic elements. Journal of the Chemical Society, Faraday Transactions. 1991;**87**(24):3881-3891

[7] Da Silva DM, Kassab LRP, Luthi SR, Araujo CB, Gomes ASL, Bell MJV. Applied Physics Letters. 2007;**90**:081913

[8] Denisov VN, Ivlev AN, Lipin AS, Mavrin BN, Orlov VG. Raman spectra and lattice dynamics of single-crystal $\alpha$-$Bi_2O_3$. Journal of Physics Condensed Matter. 1997;**9**:4967-4978

[9] De Sande JCG, Missana T, Afonso CN. Optical properties of pulsed laser deposited bismuth films. Journal of Applied Physics. 1996;**80**:7023-7027

[10] Fang J, Stokes KL, Wiemann JA, Zhou WL, Dai J, Chen F, Connor CJO. Microemulsion-processed bismuth nanoparticles. Materials Science and Engineering B. 2001;**83**:254-257

[11] Gondal MA, Saleh TA, Drmosh Q. Optical properties of bismuth oxide nanoparticles synthesized by pulsed laser ablation in liquids. Science of Advanced Materials. 2012;**4**:1-4

[12] Geng J, Hou WH, Lv YN, Zhu JJ, Chen HY. One-dimensional $BiPO_4$ nanorods and two dimensional BiOCl lamellae: Fast low temperature sonochemical synthesis, characterization, and growth mechanism. Inorganic Chemistry. 2005;**44**;8503-8509

[13] Gipson K, Kucera C, Stadther D, Stevens K, Ballato J, Brown P. The influence of synthesis parameters on particle size and photoluminescence characteristics of ligand capped $Tb^{3+}$:$LaF_3$. Polymers. 2011;**3**:2039-2052

[14] Gutierrez M, Henglein A. Nanometer sized Bi particles in aqueous solution: Absorption spectrum and some chemical properties. The Journal of Physical Chemistry. 1996; **100**:7656-7661

[15] Hardcastle FD, Wachs IE. The molecular structure of bismuth oxide by Raman spectroscopy. Journal of Solid State Chemistry. 1992;**97**:319-331

[16] Haro-Poniatowski E, Serna R, de Castro MJ, Suarez- Garcia A, Afonso CN, Vickridge I. Size dependent thermo optical properties of embedded Bi nanostructures. Nanotechnology. 2008;**19**:485708 (6 p)

[17] Hunderi O. Optical properties of metallic calcium. Journal of Physics F: Metal Physics. 1976;**6**:1223-1229

[18] Karthikeyan B, Udayabhaskar R, Kishore A. Optical and phonon properties of Sm-doped $\alpha$-$Bi_2O_3$ micro rods. Applied Physics A. 2014;**117**:1409-1414

[19] Kaur G, Rai SB. Luminescence properties of Sm, $Tb(Sal)_3Phen$ complex in polyvinyl alcohol: An approach for white-light emission. Journal of Physics D: Applied Physics. 2011;**44**:425306 (6 p)

[20] Kaur G, Dwivedi Y, Rai SB. Synthesis, structural, thermal and optical studies of rare earth coordinated complex: $Tb(Sal)_3Phen$. Materials Chemistry and Physics. 2011; **130**:1351-1356

[21] Kaur G, Dwivedi Y, Rai SB. Study of enhanced red emission from $Sm(Sal)_3Phen$ ternary complexes in Poly Vinyl Alcohol film. Optics Communication. 2010;**283**:3441-3447

[22] Kaur G, Verma RK, Rai DK, Rai SB. Plasmon-enhanced luminescence of Sm complex using silver nanoparticles in polyvinyl alcohol. Journal of Luminescence. 2012;**132**:1683-1687

[23] Kaur G. Rare Earths, Polymers and their Spectroscopy: Synthesis, Characterization, An Approach to Enhance Luminescence Intensity and Yield White light, LAP Lambert Academic Publications; 2016. 978-3-659-88306-4.

[24] Kaur G, Kumar B, Verma RK, Rai SB. Bismuth induced enhanced green emission from terbium ions and their complex in thin films. Dalton Transactions. 2014;**43**:11014-11018

[25] Kirkendall EO. Diffusion of zinc in alpha brass. Transactions of the American Institute of Mining, Metallurgical and Petroleum Engineers. 1942;**147**:104-109

[26] Kumar B, Kaur G, Singh P, Rai SB. Synthesis, structural, optical and electrical properties of metal nanoparticle–rare earth ion dispersed in polymer film. Applied Physics B. 2013;**110**:345-351

[27] Kumar B, Kaur G, Rai SB. Acetylsalicylic acid sensitized lasing luminescence of terbium complex in PVA: A case of energy avalanche via 1,10-phenanthroline. Journal of Photochemistry and Photobiology A: Chemistry. 2017;**332**:413-421

[28] Kumar B, Kaur G, Rai SB. Fluorescence quenching of $Tb^{3+}$ ions with spherical Au NPs in PVA: Structural, thermal and optical investigations. Bulletin of Laser and Spectroscopic Society of India. 81-89

[29] Kumar B, Kaur G, Singh P, Rai SB. Anomalous electrical properties of polyvinyl alcohol films with $Tb^{3+}$ ions and copper nanoparticles in different solvents. RSC Advances. 2015;**5**:1648-1654

[30] Kumari L, Lin JH, Ma YR. One dimensional $Bi_2O_3$ nanohooks: Synthesis, characterization and optical properties. Journal of Physics: Condensed Matter. 2007;**19**:406204 (11 p)

[31] Narang SN, Patel ND, Kartha VB. Infrared and Raman spectral studies and normal modes of $\alpha$-$Bi_2O_3$. Journal of Molecular Structure. 1994;**327**:221-235

[32] Perez AJS, Lopez MAC, Luckie RAM, Mendieta VS, Nunez UF, Alatorre AJ. Structural evolution of $Bi_2O_3$ prepared by thermal oxidation of bismuth nano-particles. 2005;**18**:4-8

[33] Peng M, Zollfrank C, Wondraczek L. Origin of broad NIR photoluminescence in Bismuthate glass and Bi doped glasses at room temperature. Journal of Physics: Condensed Matter. 2009;**21**:285106 (6 p)

[34] Reisfeld R, Saraidarov T. Innovative materials based on sol-gel technology. Optical Materials. 2006;**28**:64-70

[35] Reisfeld R, Pietraszkiewicz M, Saraidarov T, Levchenko V. Luminescence intensification of lanthanide complexes by silver nanoparticles incorporated in sol-gel matrix. Journal of Rare Earths. 2009;**27**;544-549

[36] Serna R, De Sande JCG, Ballesteros JM, Afonso CN. Spectroscopic ellipsometry of composite thin films with embedded Bi nanocrystals. Journal of Applied Physics. 1998;**84**:4509

[37] Sivaramakrishnan S, Muthukumar VS, Sivasankara Sai S, Venkataramaniah K, Reppert J, Rao AM, Anija M, Philip R, Kuthirummal N. Nonlinear optical scattering and absorption in bismuth nanorod suspensions. Applied Physics Letters. 2007;**91**:093104

[38] Silversmith AJ, Boye DM, Brewer KS, Gillespie CE, Lu Y, Campbell DL. $^5D_3$-$^7F_J$ emission in terbium-doped sol-gel glasses. Journal of Luminescence. 2006;**121**:14-20

[39] Talapin DV, Lee JS, Kovalenko MV, Shevchenko EV. Prospects of colloidal nanocrystals for electronic and optoelectronic applications. Chemical Reviews. 2010;**110**:389-458

[40] Toudert J, Serna R, de Castro MJ. Exploring the optical potential of nano-bismuth: Tunable surface plasmon resonances in the near ultraviolet-to-near infrared range. The Journal of Physical Chemistry C. 2012;**116**:20530-20539

[41] Wang YW, Hong BH, Kim KS. Size control of semimetal bismuth nanoparticles and the UV-visible and IR absorption spectra. The Journal of Physical Chemistry B. 2005; **109**:7067-7072

[42] Wang Q, Song F, Lin S, Ming C, Zhao H, Liu J, Zhang C, Pun EYB. Effect of silver nanoparticles with different shapes on luminescence of samarium complex at two different excitation wavelengths. Journal of Nanoparticle Research. 2011;**13**:3861-3865

[43] Wang C, Shao C, Liu Y, Zhang L. Photocatalytic properties BiOCl and $Bi_2O_3$ nanofibers prepared by electrospinning. Scripta Materialia. 2008a;**59**:332-335

[44] Wang F, Tang R, Yu H, Gibbons PC, Buhro WE. Size and shape-controlled synthesis of bismuth nanoparticles. Chemistry of Materials. 2008b;**20**:3656-3662

[45] Yu J, Wei B, Zhu L, Gao H, Sun W, Xu L. Flowerlike C-doped BiOCl nanostructures: Facile wet chemical fabrication and enhanced UV photocatalytic properties. Applied Surface Science. 2013;**284**:497-502

[46] Zhao Y, Zhang Z, Dang H. A simple way to prepare bismuth nanoparticles. Materials Letters. 2004;**58**:790-793

[47] Zhang L, Wang W, Sun S, Sun Y, Gao E, Xu J. Water splitting from dye wastewater: A case study of BiOCl/copper(II) phthalocyanine composite photocatalyst. Applied Catalysis B. 2013;**132-133**:315-320

[48] Kumar, et al. RSC Advances. 2016;**6**:26984-26992

IntechOpen